

Compress to Focus: Efficient Coordinate Compression for Policy Optimization in Multi-Turn GUI Agents

Yurun Song^{1,2,*} Jiong Yin^{1,3,*} Rongjunchen Zhang^{1,♣} Ian G. Harris²

¹HiThink Research ²University of California, Irvine ³Hangzhou Dianzi University

{yuruns, iharris}@uci.edu jiong.yin@hdu.edu.cn zhangrongjunchen@myhexin.com

Abstract

Multi-turn GUI agents enable complex task completion through sequential decision-making, but suffer from severe context inflation as interaction history accumulates. Existing strategies either sacrifice long-term context via truncation or compromise spatial structure through token pruning. In this paper, we propose Coordinate Compression Policy Optimization (CCPO), an efficient policy optimization framework that couples visual compression with policy optimization for multi-turn GUI agents. CCPO introduces Coordinate-Aware Spatial Compression (CASC), which aggregates coordinates from multiple rollouts to capture target-relevant regions and progressively narrow historical attention around key visual areas. From interactions across rollouts, CASC adaptively constructs attention boundaries that concentrate computation on the most informative regions of the scene. We further design a Distance-Based Advantage that provides fine-grained learning signals based on distance rather than binary correctness, improving both grounding accuracy and compression quality. Extensive experiments demonstrate that CCPO achieves SOTA performance across four benchmarks with up to 55% token compression and 3.8 \times training speedup. Our code can be available at <https://hithink-research.github.io/CCPO>

1 Introduction

GUI automation enables agents to execute sophisticated tasks by capturing multimodal cues. However, complex real-world workflows render single-turn interaction inadequately. Thus, effective automation requires multi-turn capabilities to execute precise decisions based on historical context.

Although multi-turn interaction facilitates complex tasks, existing GUI agents (Lu et al., 2025a;

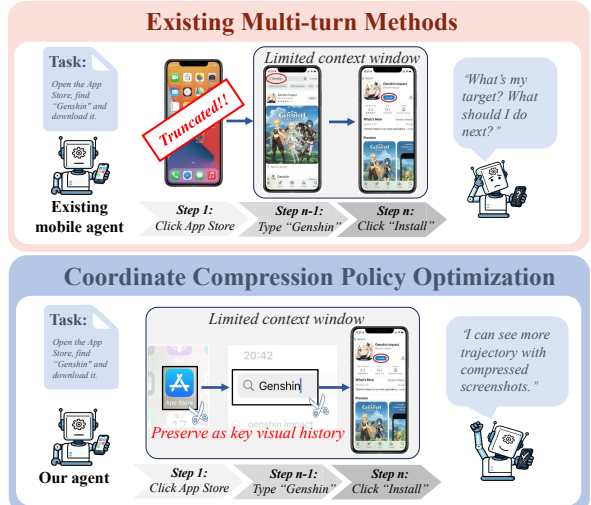


Figure 1: **Top:** Existing multi-turn methods tend to truncate the visual history due to the limited context length. **Bottom:** CCPO preserves the key visual history to maintain the longer trajectory visibility.

Chen et al., 2025; Cheng et al., 2024) struggle with context inflation. Therefore, the accumulation poses two critical challenges. First, computational costs increase rapidly as context length grows. In complex scenarios, contexts can easily exceed 32k tokens, which imposes substantial memory and latency burdens. Second, not all historical information contributes equally to current decisions. Visual tokens often contain redundancy, while naive truncation discards critical spatial information. Together, these issues motivate a selective compression approach that preserves task-critical information while filtering out irrelevant context.

To mitigate the context inflation issue, existing methods (Cheng et al., 2024; Chen et al., 2025) employ two strategies, yet both exhibit fundamental limitations in GUI scenarios. Direct truncation (Cheng et al., 2024; Lu et al., 2025a; Lin et al., 2024) aims to preserve all visual information, but it is tightly constrained by the context window, which prevents tracking long-range dependencies. Conversely, token pruning (Chen et al., 2025) summa-

* Equal contribution. Intern at HiThink Research.

♣ Corresponding Author

rizes visual context but fails to explicitly represent historical trajectories. This method disrupts the correspondence between actions and their spatial information, introducing ambiguity that hinders precise localization. Therefore, GUI agent compression faces two critical challenges: **1) Mismatch between spatial locality and temporal dependency.** While agents require long-term history for task coherence, the visual cues relevant to each decision are inherently localized around the regions where actions occur. This suggests that action trajectories should be preserved across turns, whereas retaining the full screen at every step is largely redundant. **2) Coupled optimization of compression and action policies.** Unlike static compression methods, a dynamic compression method requires foreknowledge of action-relevant regions, while accurate action prediction depends on well-compressed context. This bidirectional dependency leads to a training dilemma, as optimizing either objective alone often leads to suboptimal convergence.

In light of these insights, we propose Coordinate Compression Policy Optimization (CCPO), an efficient multi-turn policy optimization framework to couple visual compression with policy learning. The key insight of CCPO is that (i) task-relevant visual cues are spatially localized to a few critical regions, and (ii) temporal coherence is maintained by continuously tracking and preserving the trajectories of these regions over time. To this end, we introduce Coordinate-Aware Spatial Compression (CASC) to dynamically narrow attention boundaries with various action prediction. Specifically, CASC tracks interaction coordinates from predicted actions and aggregates them to compute the region of interest (ROI), then crops the visual context accordingly. This forms a virtuous cycle where improved visual focus yields better coordinate predictions, progressively tightening the spatial boundaries. Furthermore, we design the Distance-Based Advantage to replace binary feedback with smooth, distance-based supervision, thereby guiding the policy to progressively converge toward precise target locations.

Our contributions can be summarized as:

- We propose CCPO, a unified reinforcement learning framework where compression and coordinate prediction are optimized in a beneficial loop.
- We introduce Coordinate-Aware Spatial Compression, which dynamically constructs spatial attention boundaries from interaction trajectories, achieving up to 55% token reduction and $3.8 \times$

training speedup.

- We design a Distance-Based Advantage that provides soft distance-based guidance for coordinate-related actions to improve prediction accuracy and grounding abilities.
- Extensive experiments show our method achieves the state-of-the-art results on four public datasets.

2 Related Works

GUI Agents with Reinforcement Learning. Recent progress in GUI automation has been predominantly shaped by two distinct paradigms (Hu et al., 2025; Tang et al., 2025; Wang et al., 2024; Liu et al., 2025a; Wang et al., 2025b; Zhang et al., 2025b). The first generation of methods (Xu et al., 2024; Wu et al., 2024; Gou et al., 2024; Cheng et al., 2024; Gou et al., 2024; Qin et al., 2025) mainly use supervised fine-tuning on massive annotated GUI datasets, achieving strong one-step benchmark accuracy but suffering from out-of-distribution generalization and limited ability to improve through interaction with the environment. The second wave of research, motivated by the success of DeepSeek-R1 (Guo et al., 2025), has shifted toward reinforcement learning methodologies. Recent representative works (Lu et al., 2025c,b; Luo et al., 2025; Liu et al., 2025b) have adopted Group Relative Policy Optimization (GRPO) (Shao et al., 2024), achieving notable improvements in task completion rates. Yet these methods treat each action as an isolated optimization target, failing to preserve sequential dependencies crucial for multi-step task execution.

Multi-Turn Reinforcement Learning. To address the limitations of single-step optimization, recent research has explored multi-turn reinforcement learning through online environment interaction (Feng et al., 2025; Wang et al., 2025c; Dong et al., 2025; Zhang et al., 2025c). Recent approaches address multi-turn optimization through trajectory-aware curriculum learning (Shi et al., 2025), stabilized data flywheels (Wang et al., 2025a), or Semi-online RL (SO-RL) that simulates online dynamics (Lu et al., 2025c), though balancing deployment costs remains a challenge. Although these methods make progress in multi-turn optimization, they still suffer from severe context inflation.

Vision Compression in Multimodal LLMs. GUI agents suffer from computational bottlenecks due to high-resolution visual histories. Prior works address this issue via learnable query compres-

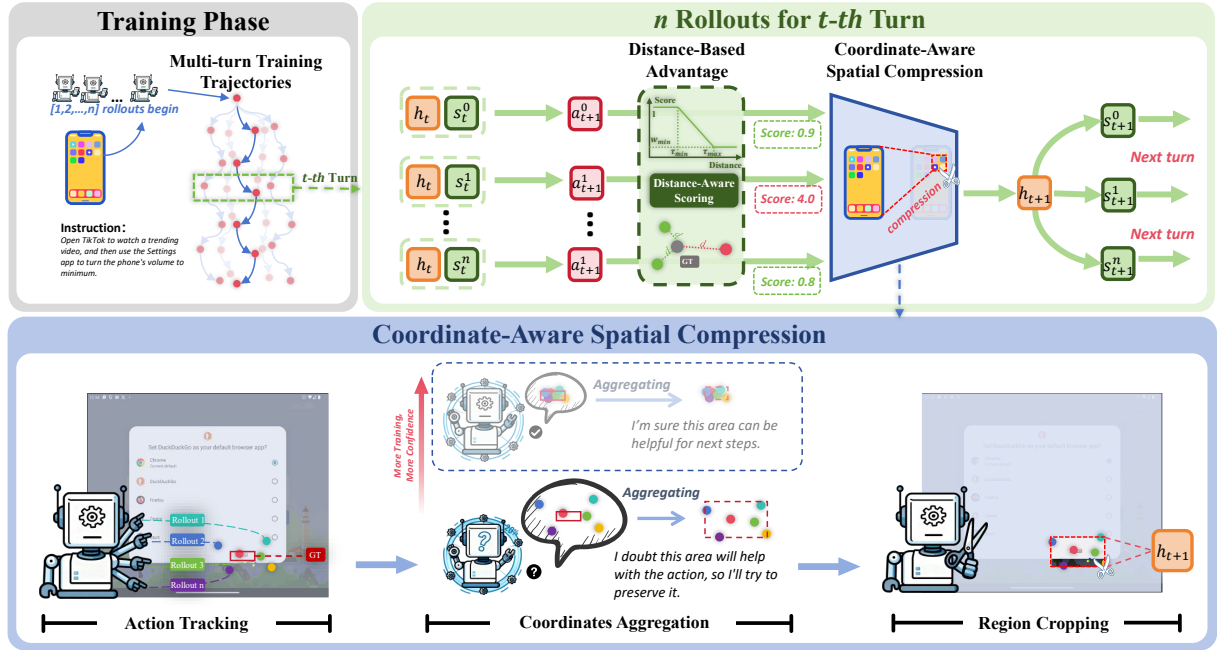


Figure 2: Overview of CCPo framework. The training phase (top) optimizes policies via multi-turn rollouts evaluated by the **Distance-Based Advantage**. The **Coordinate-Aware Spatial Compression** module (bottom) tracks n actions and aggregates coordinates to predict ROI of each step, then crops the task-relevant region as a focused visual history h_{t+1} .

sion (Hu et al., 2024; Li et al., 2023, 2024b; Zhang et al., 2025e; Zhao et al., 2025) or token pruning strategies like VoCo-LLaMA (Ye et al., 2025). However, these general-purpose methods often rely on static metrics or multi-stage training. In contrast, our CCPo couples visual compression with policy optimization, progressively focusing on the key regions to balance efficiency and grounding accuracy.

3 Method

3.1 Policy Optimization on Coordinates

In GUI agent tasks, the model needs to handle multimodal multi-turn interactions and output precise action coordinates. To better align training with task success, we move beyond standard supervised fine-tuning, in which next token prediction provides a weak signal for coordinate accuracy, as well as offline RL, which fails to consider trajectory level advantages, and traditional online RL, which is inefficient and constrained by limited data. Instead, following (Lu et al., 2025c), we use Semi-Online RL (SO-RL) by simulating online rollouts to train more efficiently while expanding the diversity of interactions.

Following the format from (Cheng et al., 2024; Chen et al., 2025), we represent interaction history using A (action-only history) and AO (action with observation history) in our work. Specifically,

nAO provides the agent with the most recent n observation frames together with the corresponding actions taken up to time t (e.g., 4AO includes the last four screenshots and their associated actions). Previous studies (Qin et al., 2025; Lu et al., 2025a; Chen et al., 2025) show that AO is more important than A because observations explicitly reveal the locality of prior actions and reduce state ambiguity.

Previous Multi-turn GUI optimization is limited by the cost of high-resolution visual tokens. Keeping full screenshot histories is inefficient, but relying only on text action traces degrades grounding and accuracy (Cheng et al., 2024; Chen et al., 2025; Lu et al., 2025a). Prior work (Chen et al., 2025; Lin et al., 2024; Zhang et al., 2025d) shows that selecting a small, and informative subset of past screenshots captures key UI changes and outperforms action-only methods, making efficient visual-history compression and selection the central challenge.

Beyond the memory and computation required to maintain a long visual history, accurate coordinate prediction is another major challenge. Because most GUI actions are coordinate-based ($> 70\%$) shown in Figure 5, accurate point prediction is essential for correct steps, reliable grounding, and overall task success. Small localization errors can cause misclicks, unintended UI changes, and disrupt the interaction flow.

Therefore, we focus on GUI grounding while reducing long-horizon costs by concentrating computation on high-confidence ROI through coordinate sampling. As shown in Figure 2, our approach Coordinate Compression Policy Optimization (CCPO) has three core components: Progressive Rollout Trajectory, Coordinate-Aware Spatial Compression, and Distance-Based Advantage.

3.2 Progressive Rollout Trajectory

We consider a GUI environment in which an agent is given a high-level instruction I and interacts with the interface over a horizon of T steps. At each step $t \in \{1, \dots, T\}$, the agent observes a screenshot s_t and executes an action prediction a_t , while a_t^* represents a corresponding annotated action. The interaction history up to step t is defined as

$$h_t = \{(s_1, a_1), (s_2, a_2), \dots, (s_{t-1}, a_{t-1})\} \quad (1)$$

An annotated trajectory is given by

$$\tau^* = \{(s_1, a_1^*), (s_2, a_2^*), \dots, (s_T, a_T^*)\} \quad (2)$$

During training, we sample N rollouts from the current policy π where $i = 1, \dots, N$ denotes the i -th rollout trajectory. Each action from rollout is associated with coordinates or other auxiliary information, denoted by $c_t^{(i)}$, we define the coordinate-augmented history as

$$ch_t = \{(\tilde{s}_k, \{a_k^{(i)}, c_k^{(i)}\}_{i=1}^N)\}_{k=1}^{t-1} \quad (3)$$

where $c_t^{(i)}$ can be \emptyset , depending on the action type, and \tilde{s}_t denotes the screenshot after the processing from coordinates $c_{t-1}^0, \dots, c_{t-1}^i$. ch_t is the t -th history shared across N rollouts for different τ_t . For a given turn t , the entire rollout trajectory, for $i = 1, \dots, N$, is

$$\tau_t = \{ch_t, \{(s_t^1, a_t^1), (s_t^2, a_t^2), \dots, (s_t^i, a_t^i)\}\} \quad (4)$$

At step t in rollout i , the policy π produces the next action conditioned on the coordinate-augmented history:

$$a_t^{(i)} \sim \pi(\cdot \mid I, s_t^{(i)}, ch_t). \quad (5)$$

In our multi-turn RL environment, if the annotated trajectory contains a coordinate-related action, we proceed as follows during training: we sample N rollouts, each consisting of N actions. Whenever an action prediction in any rollout produces coordinates, we record those coordinates as historical

coordinates. After each rollout, to construct a robust attention boundary that covers potential ROI, we aggregate all coordinates from that rollout together with annotated coordinate from training data. In the next generation round, we crop the input images based on the aggregated historical coordinates collected from the previous sampling round.

The Progressive Rollout strategy offers two key benefits: (i) it enables cross-rollout learning, since all rollouts share the same coordinate history, improving consistency and exploration. (ii) it progressively refines this history, as each turn adds context around the annotated and predicted coordinates. This yields a confident ROI over the image derived from accumulated sampling.

3.3 Coordinate-Aware Spatial Compression

To enable the preservation of interaction histories within a limited context window, our CASC keeps the key visual information associated with coordinate-related actions, discarding all other historical images to achieve maximum compression.

Each action has a type and auxiliary details:

$$a_t^{(i)} = (u_t^{(i)}, z_t^{(i)}), \quad (6)$$

where $u_t^{(i)} \in \mathcal{U}$ is the action type (e.g., click, type, wait), and $z_t^{(i)} \in \mathcal{Z}$ are auxiliary details (coordinates, text, time, etc.).

For general coordinate compression, we categorize actions into the following groups:

Coordinate-related actions \mathcal{A}_{wc} : actions such as click, long-press, select and scroll. These actions carry essential coordinate information for localization and are useful for our CASC. We treat scroll as a coordinate action in our work.

Non-coordinate actions \mathcal{A}_{nc} : actions such as type, wait, open, and complete. These actions do not require coordinate prediction, and we remove their corresponding images from the trajectory.

CASC consists of three main components that work together across multi-turn rollouts.

1. **Action Tracking:** This component records coordinate-based actions across turns and rollouts by tracking prior model outputs, annotated actions, and coordinate bounding boxes if present. It maintains a trajectory coordinate history for efficient reuse in later rounds.

$$\mathcal{C}_t = \left\{ c_t^{(i)} \mid a_t^{(i)} \in \mathcal{A}_{wc}; t = 1, \dots, T \right\} \quad (7)$$

2. **Coordinate Aggregation:** Once coordinates have been collected, the aggregation component

groups them by rollouts. It then converts the set of coordinate candidates into a single aggregated bounding box that defines a useful ROI for image history.

$$\mathcal{C}_t^{\text{anot}} = \{ c_t^* \mid a_t^* \in \mathcal{A}_{wc}; t = 1, \dots, T \} \quad (8)$$

The aggregated historical coordinate set, shared across rollouts for the next round, is then

$$\mathcal{C}_t^{\text{hist}} = c_t^* \cup \{c_t^1, \dots, c_t^{(i)}\} \quad (9)$$

3. Region Cropping: For each historical step, the ROI bounding boxes are used to crop the corresponding image regions. These cropped regions then act as compressed image history for subsequent rounds of generation.

$$\tilde{S}_t = \text{Crop}(S_t; \mathcal{C}_t^{\text{hist}}) \quad (10)$$

where $\text{Crop}(\cdot; \mathcal{C}_t^{\text{hist}})$ is an operator that crops the screenshot based on the aggregated historical coordinates $\mathcal{C}_t^{\text{hist}}$.

By dynamically filtering out irrelevant visual redundancy while preserving task-critical context, CASC establishes a virtuous cycle where focused visual history progressively refines coordinate prediction accuracy. This approach significantly alleviates context inflation, enabling the efficient processing of interactions while maintaining precise spatial grounding.

3.4 Distance-Based Advantage

To provide fine-grained supervision that guides the policy toward precise locations, we design a step-level distance-based advantage. Specifically, in order to improve the grounding abilities, we use

$$r_t = \alpha \cdot r_{\text{format}} + \beta \cdot r_{\text{type}} + \gamma \cdot r_{\text{acc}} \quad (11)$$

Format Reward Use r_{format} to denote a binary reward: r_{format} is 1 if the response follows the required format (e.g., `<action>` tag) and 0 otherwise.

Action Type Reward Use r_{type} to denote a binary reward: assign 1 if $\hat{u} = u^*$, and 0 otherwise.

Coordinate-Aware Reward (CR) Let $\hat{\mathbf{c}}$ be the predicted normalized coordinate, \mathbf{c} the ground-truth normalized coordinate, and \mathcal{B} the ground-truth bounding box. The normalized distance is

$$d_{\text{norm}}(\hat{\mathbf{c}}, \mathbf{c}) = \|\hat{\mathbf{c}} - \mathbf{c}\|_2 \quad (12)$$

where $\hat{\mathbf{c}}, \mathbf{c} \in [0, 1]$ and $d_{\text{norm}} \in [0, \sqrt{2}]$. Let τ_{\min} be the normalized tolerance threshold τ_{\max} the normalized maximum tolerance, and w_{\min} the minimum weight that given only when r_{format} and r_{type}

are correct. The coordinate accuracy reward is

$$r_{\text{acc}}(\hat{\mathbf{c}}, \mathbf{c}, \mathcal{B}) = \begin{cases} 1, & d_{\text{norm}} \leq \tau_{\min} \\ w_{\min}, & d_{\text{norm}} \geq \tau_{\max} \\ 1 - \frac{d_{\text{norm}} - \tau_{\min}}{\tau_{\max} - \tau_{\min}} (1 - w_{\min}), & \tau_{\min} < d_{\text{norm}} < \tau_{\max} \end{cases}$$

The coordinate reward function is applied only when $a_{\text{type}} \in \mathcal{A}_{wc}$. For non-coordinate actions, the accuracy reward is binary:

$$r_{\text{acc}}(\hat{a}, a^*) = \begin{cases} 1, & \text{if } (\hat{u}, \hat{z}) = (u^*, z^*) \\ 0, & \text{otherwise.} \end{cases} \quad (13)$$

Applying the coordinate-dependent advantage at the step level has two main benefits: (i) It improves performance by providing a smoother and more informative training reward instead of a hard binary reward. This is especially important given that more than half of the predictions correspond to actions with coordinates. (ii) It encourages the model to predict spatially coherent coordinates concentrated on target-relevant regions, rather than dispersed points, enabling more effective compression of long visual histories.

4 Experiments

4.1 Datasets

We train and evaluate our models on four widely used datasets for GUI agent tasks, described below.

Dataset	Domain	Task	Steps
AITW	Mobile & Web	2,939	8.1
Mind2Web	Web	2,350	7.3
GUI-Odyssey	Mobile	7,735	15.4
AndroidControl	Mobile	15,283	5.5

Table 1: Dataset statistics for the AITW (Rawles et al., 2023), Mind2Web (Deng et al., 2023), GUI-Odyssey (Lu et al., 2025a), and AndroidControl (Li et al., 2024a) datasets, including domain, number of tasks, and average task length (in steps).

4.2 Experiments Setup

Our experiments focus on three settings: (i) SFT (ii) Semi-online RL from (Lu et al., 2025c) (iii) SFT followed by CCPO. We do not preprocess the resolution of the original screenshots. Instead, we follow the (Lu et al., 2025c) and use the same maximum pixel budget. We use a history length of 3AO as the default experimental setting unless otherwise specified. For the SFT part, we report the best

Model	History Format AOT	Android Control			High			GUI Odyssey		
		TM	GR	SR	TM	GR	SR	TM	GR	SR
<i>Open-source Models</i>										
OS-Atlas-4B ZS (Wu et al., 2024)	A	49.0	49.5	22.8	49.6	34.6	20.3			
OS-Atlas-4B FT (Wu et al., 2024)	A	84.7	73.8	67.5	83.5	61.4	56.4			
Qwen2.5VL-3B (Bai et al., 2025)	A	47.8	46.5	38.9	37.4	26.5	26.7			
UI-R1-3B (Lu et al., 2025b)	—	57.9	55.7	45.4	52.2	34.5	32.5			
GUI-R1-3B (Luo et al., 2025)	A	58.0	56.2	46.6	54.8	41.5	41.3			
OS-Genesis-7B (Sun et al., 2025)	AO	65.9	—	44.4	11.7	—	3.6			
Aguvis-7B (Xu et al., 2024)	A	65.6	—	54.2	26.7	—	13.5			
GUI-R1-7B (Luo et al., 2025)	A	71.6	65.6	51.7	65.5	43.6	38.8			
AgentCPM-GUI-8B (Zhang et al., 2025f)	A	77.7	—	69.2	90.8	—	75.0			
OS-Atlas-7B ZS (Wu et al., 2024)	A	57.4	54.9	29.8	60.4	39.7	27.0			
OS-Atlas-7B FT (Wu et al., 2024)	A	85.2	78.5	71.2	84.5	67.8	62.0			
UI-TARS-7B (Qin et al., 2025)	AOT	83.7	80.5	<u>72.5</u>	94.6	90.1	87.0			
UI-S1-7B (Lu et al., 2025c)	AOT	79.9	73.4	68.2	76.3	61.7	59.5			
<i>Our Models</i>										
Qwen2.5VL-3B (0-shot)	AO	24.9	68.3	20.2	27.8	46.4	14.7			
w/ SFT	AO	85.2	73.5	68.6	88.0	84.3	75.9			
w/ Semi-online RL	AO	83.7	74.8	67.5	82.6	81.3	71.3			
CCPO-3B-1AO	AO	85.3	76.7	70.6	91.7	87.2	81.1			
CCPO-3B-3AO	AO	85.7	77.5	70.8	90.6	88.5	80.9			
Qwen2.5VL-7B (0-shot)	AO	58.9	70.3	44.4	55.8	50.8	31.8			
w/ SFT	AO	85.9	75.9	70.6	88.0	84.6	76.0			
w/ Semi-online RL	AO	86.3	76.7	70.6	89.2	84.9	76.7			
CCPO-7B-1AO	AO	<u>86.5</u>	78.8	72.2	91.1	87.2	80.3			
CCPO-7B-3AO	AO	86.9	<u>79.7</u>	73.3	91.8	89.3	82.4			

Table 2: Results of CCPO on the Android Control and GUI-Odyssey. We report type matching (TM), grounding rate (GR), and success rate (SR). For the history format, AOT denotes Action, Observation, and Thought histories, respectively.

checkpoint and configuration to ensure fairness. More details can be found in the Appendix A.1.

4.3 Baseline Models

Following prior work, we use Qwen2.5-VL 3B and Qwen2.5-VL 7B as our base models for both SFT and reinforcement learning. We compare our approach against a broad range of existing methods from two perspectives: (i) General-purpose GUI agents that are commonly used in prior studies, like (Xu et al., 2024; Sun et al., 2025; Wu et al., 2024; Qin et al., 2025; Lu et al., 2025c). (ii) Specialized models designed to improve GUI agent efficiency, such as (Cheng et al., 2024; Ge et al., 2025; Lin et al., 2024; Chen et al., 2025).

5 Main Results

5.1 GUI Benchmark

Android Control Table 2 shows that adding 3AO history with CCPO delivers state-of-the-art results on Android Control (AC) for our 7B model. Specifically, it provides 3.2% TM and 0.8% SR improvement over UI-TARS-7B. Compared to the 1AO

variant, it improves TM by 0.4%, GR by 0.9%, and SR by 1.1%. It also outperforms SFT and Semi-online RL by increasing 3–4% GR and 2–3% SR, demonstrating consistent gains over prior work and our baselines on the AC dataset.

GUI Odyssey Table 2 shows that our 3B model achieves substantial improvements over UI-S1 with gains of 15.5%, 27.6%, 22.9% in TM, GR and SR with 3AO history on GUI Odyssey dataset. Compared to the 1AO variant, CCPO outperforms by 14.8% in TM, 25.5% in GR, and 20.8% in SR. These results confirm that CCPO generalizes well to cross-app navigation scenarios with longer average trajectories.

Mind2Web Table 3 reports Mind2Web (M2W) results, where CCPO consistently outperforms SFT and prior baselines at both 3B and 7B models. CCPO-7B-3AO surpasses TongUI-7B by 6.1% on Cross-Task, 4.7% on Cross-Website, and 3.6% on Cross-Domain, while CCPO-3B exceeds SimpAgent by 7.8%, 8.8%, and 6.8%, respectively. Full results are provided in Appendix 18.

AITW Table 3 summarizes Android in the Wild

Method	Param	Mind2Web			AITW	
		Cross-Task	Cross-Website	Cross-Domain	Overall	ClickAvg
Qwen-VL 9.6B (Bai et al., 2023)	9.6B	13.3	9.2	12.0	54.3	57.4
SeeClick (Cheng et al., 2024)	9.6B	25.5	16.4	20.8	59.3	66.4
R-VLM (Park et al., 2025)	9.6B	28.7	26.1	24.3	64.9	71.0
Iris (Ge et al., 2025)	9.6B	32.0	26.2	28.8	63.6	71.0
Qwen2-VL (Bai et al., 2025)	2B	46.7	42.2	44.6	57.7	—
ShowUI-2B (Lin et al., 2024)	2B	37.2	35.1	35.2	70.0	—
SimpAgent (Chen et al., 2025)	2B	48.7	42.2	45.0	71.5	—
TongUI-3B (Zhang et al., 2025a)	3B	48.8	48.1	49.5	71.6	—
TongUI-7B (Zhang et al., 2025a)	7B	53.4	49.0	52.9	73.3	—
Qwen2.5-VL-3B w/ SFT	3B	52.0	46.5	48.7	70.8	78.4
CCPO-3B 1AO	3B	54.6	50.7	50.6	71.8	79.7
CCPO-3B 3AO	3B	56.5	51.0	51.8	73.1	80.4
Qwen2.5-VL-7B w/ SFT	7B	55.6	51.3	52.0	72.3	80.2
CCPO-7B-1AO	7B	58.0	53.4	55.7	73.5	81.0
CCPO-7B-3AO	7B	59.5	53.7	56.5	74.4	81.4

Table 3: Results of CCPO on the Mind2Web and AITW benchmarks across different settings.

Model	History Length	Token Length \downarrow	Compression Rate \uparrow	Training Time (s/step) \downarrow
SO-RL-3B	1AO	6998	0.0%	515
	3AO	9888	0.0%	660
CCPO-3B	1AO	4271	38.9% (3.3 \times)	154 (3.3 \times)
	3AO	4460	54.9% (3.8 \times)	174 (3.8 \times)
SO-RL-7B	1AO	7026	0.0%	569
	3AO	9550	0.0%	717
CCPO-7B	1AO	4262	39.3% (3.1 \times)	186 (3.1 \times)
	3AO	4473	53.2% (3.5 \times)	204 (3.5 \times)

Table 4: Training efficiency comparison between CCPO and Semi-online RL on the Android Control dataset.

(AITW) results, where CCPO shows consistent gains. CCPO-7B-3AO improves over CCPO-7B-1AO by 0.9% and exceeds TongUI by 1.1%, while CCPO-3B-3AO outperforms CCPO-3B-1AO by 1.3%. Detailed results are in Appendix 17.

5.2 AO Length Scaling

Figure 3 shows how performance changes on the AITW dataset as the AO length increases from 1AO to 5AO. For the SFT baseline, extending the AO length from 1AO to 5AO improves accuracy by an average of 1.8% across five subtasks. A similar pattern is observed for CCPO that 3AO consistently outperforms 1AO and 2AO, and overall accuracy improves by 1.7%. Overall, longer AO history leads to better results for both SFT and CCPO. Detailed results are reported in Table 16.

5.3 Training Efficiency

Table 4 presents the training efficiency comparison between our method and Semi-online RL on Android Control dataset. Specifically, CCPO-7B compresses the token length to 39.3%–53.2% of the original in terms of 1AO and 3AO, corresponding to training speedups of 3.1 \times and 3.5 \times under 1AO and 3AO settings, respectively. Moreover, CCPO-3B achieves even greater speedups of 3.3 \times and 3.8 \times while maintaining comparable token efficiency, making it suitable for resource-constrained scenarios. Notably, as the history length increases from 1AO to 3AO, the token length in Semi-online RL grows by 41%, while our method maintains a relatively stable token length with only a 4% increase. This demonstrates that our compres-

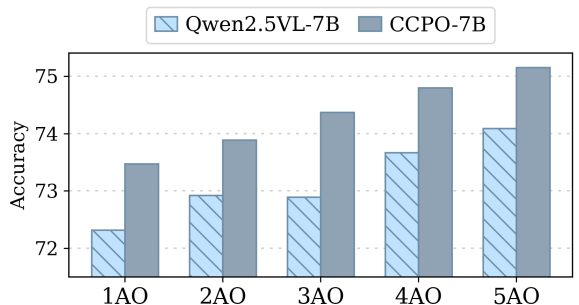


Figure 3: Performance comparison for different AO on AITW dataset.

Method	AC-TM	AC-GR	AC-SR
Qwen2.5VL-7B SFT	85.94	75.95	70.60
+ Semi-online	86.27 (+0.33)	77.93 (+1.98)	72.35 (+1.75)
+ CASC	86.72 (+0.78)	79.12 (+3.17)	72.70 (+2.1)
+ CASC + CR	86.89 (+0.95)	79.71 (+3.76)	73.25 (+2.65)

Table 5: Ablation study of different components on the Android Control dataset.

sion strategy scales efficiently with longer action-observation histories. More details are available in Appendix A.6

6 Analysis

6.1 Component Ablation

Table 5 validates the contribution of each CCPo module on the Android Control dataset. It can be observed that CASC leads to a substantial improvement in Grounding Rate, indicating that suppressing visual redundancy mitigates spatial ambiguity and enhances attention toward task-relevant regions. The Coordinate-Aware Reward further enhances overall performance by leveraging fine-grained, distance-based supervision to achieve superior coordinate precision.

6.2 Computational Overhead Analysis

Table 6 shows a fine-grained profiling of the computational overhead. Specifically, a 44% reduction in compute load means it requires significantly fewer computational resources. To quantify the wall-clock speedup, we measure *token latency* (average time per token) and *step latency* (time per training step). In these metrics, we observe a 10% reduction in token latency and a 35% decrease in step latency. These results confirm that CCPo effectively reduces training time while maintaining comparable performance.

Method	Compute Load (TFLOPS) \downarrow	Token Latency (ms) \downarrow	Step Latency (s) \downarrow
SO-RL	9.6	0.064	297.1
CCPO	5.4 (-44%)	0.057 (-10%)	194.5 (-35%)

Table 6: Training efficiency comparison in terms of compute load and latency.

6.3 Qualitative Analysis

Figure 4 visualizes the attention maps of the SFT baseline and our CCPo method on the same GUI screenshot. The SFT model in Figure 4 (a) shows scattered attention across the entire screen, while



Figure 4: Attention maps between SFT and CCPo. CCPo accurately predicts actions and localizes coordinates, with stronger focus on detailed historical context and key elements.

CCPO in Figure 4 (b) exhibits concentrated attention on task-relevant regions. This demonstrates that our coordinate-based compression effectively guides the model to focus on interaction areas, thereby improving coordinate prediction accuracy and reducing computational overhead from processing irrelevant visual tokens.

7 Conclusion

We introduce Coordinate Compression Policy Optimization (CCPO), an efficient policy optimization framework for GUI agents that progressively refines attention over multiple rollouts. CCPO uses Coordinate-Aware Spatial Compression (CASC) to focus on task-relevant regions from long action-observation histories. By compressing irrelevant areas, it achieves a high compression rate and substantially improves computational efficiency. We also propose Distance-Based Advantage that guides policies smoothly toward target locations instead of relying on hard thresholds. Together, these designs enable more efficient training and stronger multi-turn decision making. CCPO achieves state-of-the-art results on diverse GUI benchmarks with fewer training resources, making it a practical and resource-efficient approach for future GUI agents.

References

Jinze Bai, Shuai Bai, Yunfei Chu, Zeyu Cui, Kai Dang, Xiaodong Deng, Yang Fan, Wenbin Ge, Yu Han, Fei Huang, and 1 others. 2023. Qwen technical report. *arXiv preprint arXiv:2309.16609*.

Shuai Bai, Keqin Chen, Xuejing Liu, Jialin Wang, Wenbin Ge, Sibo Song, Kai Dang, Peng Wang, Shijie Wang, Jun Tang, and 1 others. 2025. Qwen2. 5-vl technical report. *arXiv preprint arXiv:2502.13923*.

Gongwei Chen, Xurui Zhou, Rui Shao, Yibo Lyu, Kaiwen Zhou, Shuai Wang, Wentao Li, Yinchuan Li, Zhongang Qi, and Liqiang Nie. 2025. Less is more: Empowering gui agent with context-aware simplification. In *Proceedings of the IEEE/CVF International Conference on Computer Vision*, pages 5901–5911.

Kanzhi Cheng, Qiushi Sun, Yougang Chu, Fangzhi Xu, Yantao Li, Jianbing Zhang, and Zhiyong Wu. 2024. Seeclick: Harnessing gui grounding for advanced visual gui agents. *arXiv preprint arXiv:2401.10935*.

Xiang Deng, Yu Gu, Boyuan Zheng, Shijie Chen, Samuel Stevens, Boshi Wang, Huan Sun, and Yu Su. 2023. [Mind2web: Towards a generalist agent for the web](#). *Preprint*, arXiv:2306.06070.

Guanting Dong, Hangyu Mao, Kai Ma, Licheng Bao, Yifei Chen, Zhongyuan Wang, Zhongxia Chen, Jiazheng Du, Huiyang Wang, Fuzheng Zhang, and 1 others. 2025. Agentic reinforced policy optimization. *arXiv preprint arXiv:2507.19849*.

Lang Feng, Zhenghai Xue, Tingcong Liu, and Bo An. 2025. Group-in-group policy optimization for Ilm agent training. *arXiv preprint arXiv:2505.10978*.

Zhiqi Ge, Juncheng Li, Xinglei Pang, Minghe Gao, Kaihang Pan, Wang Lin, Hao Fei, Wenqiao Zhang, Siliang Tang, and Yueling Zhuang. 2025. Iris: Breaking gui complexity with adaptive focus and self-refining. In *Proceedings of the IEEE/CVF International Conference on Computer Vision*, pages 24559–24568.

Boyu Gou, Ruohan Wang, Boyuan Zheng, Yanan Xie, Cheng Chang, Yiheng Shu, Huan Sun, and Yu Su. 2024. Navigating the digital world as humans do: Universal visual grounding for gui agents. *arXiv preprint arXiv:2410.05243*.

Daya Guo, Dejian Yang, Haowei Zhang, Junxiao Song, Ruoyu Zhang, Runxin Xu, Qihao Zhu, Shirong Ma, Peiyi Wang, Xiao Bi, and 1 others. 2025. Deepseek-r1: Incentivizing reasoning capability in Ilms via reinforcement learning. *arXiv preprint arXiv:2501.12948*.

Wenyi Hong, Weihan Wang, Qingsong Lv, Jiazheng Xu, Wenmeng Yu, Junhui Ji, Yan Wang, Zihan Wang, Yuxiao Dong, Ming Ding, and 1 others. 2024. Cogagent: A visual language model for gui agents. In *Proceedings of the IEEE/CVF Conference on Computer Vision and Pattern Recognition*, pages 14281–14290.

Wenbo Hu, Yifan Xu, Yi Li, Weiyue Li, Zeyuan Chen, and Zhuowen Tu. 2024. Bliva: A simple multimodal Ilm for better handling of text-rich visual questions. In *Proceedings of the AAAI Conference on Artificial Intelligence*, volume 38, pages 2256–2264.

Xueyu Hu, Tao Xiong, Biao Yi, Zishu Wei, Ruixuan Xiao, Yurun Chen, Jiasheng Ye, Meiling Tao, Xiangxin Zhou, Ziyu Zhao, and 1 others. 2025. Os agents: A survey on mllm-based agents for general computing devices use. *arXiv preprint arXiv:2508.04482*.

Junnan Li, Dongxu Li, Silvio Savarese, and Steven Hoi. 2023. Blip-2: Bootstrapping language-image pre-training with frozen image encoders and large language models. In *International conference on machine learning*, pages 19730–19742. PMLR.

Wei Li, William Bishop, Alice Li, Chris Rawles, Folawiyo Campbell-Ajala, Divya Tyamagundlu, and Oriana Riva. 2024a. On the effects of data scale on computer control agents. *arXiv preprint arXiv:2406.03679*.

Yanwei Li, Chengyao Wang, and Jiaya Jia. 2024b. Llama-vid: An image is worth 2 tokens in large language models. In *European Conference on Computer Vision*, pages 323–340. Springer.

Kevin Qinghong Lin, Linjie Li, Difei Gao, Zhengyuan Yang, Zechen Bai, Weixian Lei, Lijuan Wang, and Mike Zheng Shou. 2024. Showui: One vision-language-action model for generalist gui agent. In *NeurIPS 2024 Workshop on Open-World Agents*, volume 1.

Guangyi Liu, Pengxiang Zhao, Liang Liu, Yaxuan Guo, Han Xiao, Weifeng Lin, Yuxiang Chai, Yue Han, Shuai Ren, Hao Wang, and 1 others. 2025a. Llm-powered gui agents in phone automation: Surveying progress and prospects. *arXiv preprint arXiv:2504.19838*.

Yuhang Liu, Pengxiang Li, Congkai Xie, Xavier Hu, Xiaotian Han, Shengyu Zhang, Hongxia Yang, and Fei Wu. 2025b. Infigui-r1: Advancing multimodal gui agents from reactive actors to deliberative reasoners. *arXiv preprint arXiv:2504.14239*.

Quanfeng Lu, Wenqi Shao, Zitao Liu, Lingxiao Du, Fanqing Meng, Boxuan Li, Botong Chen, Siyuan Huang, Kaipeng Zhang, and Ping Luo. 2025a. Guiodyssey: A comprehensive dataset for cross-app gui navigation on mobile devices. In *Proceedings of the IEEE/CVF International Conference on Computer Vision*, pages 22404–22414.

Zhengxi Lu, Yuxiang Chai, Yaxuan Guo, Xi Yin, Liang Liu, Hao Wang, Guanjing Xiong, and Hongsheng Li. 2025b. Ui-r1: Enhancing action prediction of gui agents by reinforcement learning. *CoRR*.

Zhengxi Lu, Jiabo Ye, Fei Tang, Yongliang Shen, Haiyang Xu, Ziwei Zheng, Weiming Lu, Ming Yan, Fei Huang, Jun Xiao, and 1 others. 2025c. Ui-s1:

Advancing gui automation via semi-online reinforcement learning. *arXiv preprint arXiv:2509.11543*.

Run Luo, Lu Wang, Wanwei He, and Xiaobo Xia. 2025. Gui-r1: A generalist r1-style vision-language action model for gui agents. *arXiv preprint arXiv:2504.10458*.

Joonhyung Park, Peng Tang, Sagnik Das, Srikanth Apalaraju, Kunwar Yashraj Singh, R Manmatha, and Shabnam Ghadar. 2025. R-vlm: Region-aware vision language model for precise gui grounding. In *Findings of the Association for Computational Linguistics: ACL 2025*, pages 9669–9685.

Yujia Qin, Yining Ye, Junjie Fang, Haoming Wang, Shihao Liang, Shizuo Tian, Junda Zhang, Jiahao Li, Yunxin Li, Shijue Huang, and 1 others. 2025. Utars: Pioneering automated gui interaction with native agents. *arXiv preprint arXiv:2501.12326*.

Christopher Rawles, Alice Li, Daniel Rodriguez, Oriana Riva, and Timothy Lillicrap. 2023. Androidinthewild: A large-scale dataset for android device control. *Advances in Neural Information Processing Systems*, 36:59708–59728.

Zhihong Shao, Peiyi Wang, Qihao Zhu, Runxin Xu, Junxiao Song, Xiao Bi, Haowei Zhang, Mingchuan Zhang, YK Li, Yang Wu, and 1 others. 2024. Deepseekmath: Pushing the limits of mathematical reasoning in open language models. *arXiv preprint arXiv:2402.03300*.

Yucheng Shi, Wenhao Yu, Zaitang Li, Yonglin Wang, Hongming Zhang, Ninghao Liu, Haitao Mi, and Dong Yu. 2025. Mobilegui-rl: Advancing mobile gui agent through reinforcement learning in online environment. *arXiv preprint arXiv:2507.05720*.

Qiushi Sun, Kanzhi Cheng, Zichen Ding, Chuanyang Jin, Yian Wang, Fangzhi Xu, Zhenyu Wu, Chengyou Jia, Liheng Chen, Zhoumianze Liu, and 1 others. 2025. Os-genesis: Automating gui agent trajectory construction via reverse task synthesis. In *Proceedings of the 63rd Annual Meeting of the Association for Computational Linguistics (Volume 1: Long Papers)*, pages 5555–5579.

Fei Tang, Haolei Xu, Hang Zhang, Siqi Chen, Xingyu Wu, Yongliang Shen, Wenqi Zhang, Guiyang Hou, Zeqi Tan, Yuchen Yan, and 1 others. 2025. A survey on (m) llm-based gui agents. *arXiv preprint arXiv:2504.13865*.

Haoming Wang, Haoyang Zou, Huatong Song, Jiazhan Feng, Junjie Fang, Junting Lu, Longxiang Liu, Qinyu Luo, Shihao Liang, Shijue Huang, and 1 others. 2025a. Ui-tars-2 technical report: Advancing gui agent with multi-turn reinforcement learning. *arXiv preprint arXiv:2509.02544*.

Shuai Wang, Weiwen Liu, Jingxuan Chen, Yuqi Zhou, Weinan Gan, Xingshan Zeng, Yuhan Che, Shuai Yu, Xinlong Hao, Kun Shao, and 1 others. 2024. Gui agents with foundation models: A comprehensive survey. *arXiv preprint arXiv:2411.04890*.

Xinyuan Wang, Bowen Wang, Dunjie Lu, Junlin Yang, Tianbao Xie, Junli Wang, Jiaqi Deng, Xiaole Guo, Yiheng Xu, Chen Henry Wu, and 1 others. 2025b. Opencua: Open foundations for computer-use agents. *arXiv preprint arXiv:2508.09123*.

Zihan Wang, Kangrui Wang, Qineng Wang, Pingyue Zhang, Linjie Li, Zhengyuan Yang, Xing Jin, Kefan Yu, Minh Nhat Nguyen, Licheng Liu, and 1 others. 2025c. Ragen: Understanding self-evolution in llm agents via multi-turn reinforcement learning. *arXiv preprint arXiv:2504.20073*.

Zhiyong Wu, Zhenyu Wu, Fangzhi Xu, Yian Wang, Qiushi Sun, Chengyou Jia, Kanzhi Cheng, Zichen Ding, Liheng Chen, Paul Pu Liang, and 1 others. 2024. Os-atlas: A foundation action model for generalist gui agents. *arXiv preprint arXiv:2410.23218*.

Yiheng Xu, Zekun Wang, Junli Wang, Dunjie Lu, Tianbao Xie, Amrita Saha, Doyen Sahoo, Tao Yu, and Caiming Xiong. 2024. Aguvis: Unified pure vision agents for autonomous gui interaction. *arXiv preprint arXiv:2412.04454*.

Xubing Ye, Yukang Gan, Xiaoke Huang, Yixiao Ge, and Yansong Tang. 2025. Voco-llama: Towards vision compression with large language models. In *Proceedings of the Computer Vision and Pattern Recognition Conference*, pages 29836–29846.

Bofei Zhang, Zirui Shang, Zhi Gao, Wang Zhang, Rui Xie, Xiaojian Ma, Tao Yuan, Xinxiao Wu, Song-Chun Zhu, and Qing Li. 2025a. Tongui: Building generalized gui agents by learning from multimodal web tutorials. *arXiv preprint arXiv:2504.12679*.

Chi Zhang, Zhao Yang, Jiaxuan Liu, Yanda Li, Yucheng Han, Xin Chen, Zebiao Huang, Bin Fu, and Gang Yu. 2025b. Appagent: Multimodal agents as smartphone users. In *Proceedings of the 2025 CHI Conference on Human Factors in Computing Systems*, pages 1–20.

Guibin Zhang, Hejia Geng, Xiaohang Yu, Zhenfei Yin, Zaibin Zhang, Zelin Tan, Heng Zhou, Zhongzhi Li, Xiangyuan Xue, Yijiang Li, and 1 others. 2025c. The landscape of agentic reinforcement learning for llms: A survey. *arXiv preprint arXiv:2509.02547*.

Jiwen Zhang, Ya-Qi Yu, Minghui Liao, Wentao Li, Jihao Wu, and Zhongyu Wei. 2025d. Ui-hawk: Unleashing the screen stream understanding for mobile gui agents. In *Proceedings of the 2025 Conference on Empirical Methods in Natural Language Processing*, pages 18228–18247.

Renshan Zhang, Rui Shao, Gongwei Chen, Miao Zhang, Kaiwen Zhou, Weili Guan, and Liqiang Nie. 2025e. Falcon: Resolving visual redundancy and fragmentation in high-resolution multimodal large language models via visual registers. *arXiv preprint arXiv:2501.16297*.

Zhong Zhang, Yaxi Lu, Yikun Fu, Yupeng Huo, Shen-zhi Yang, Yesai Wu, Han Si, Xin Cong, Haotian

Chen, Yankai Lin, and 1 others. 2025f. Agentcpm-gui: Building mobile-use agents with reinforcement fine-tuning. *arXiv preprint arXiv:2506.01391*.

Zhiqian Zhao, Liang Li, Jiehua Zhang, Yaoqi Sun, Xichun Sheng, Haibing Yin, and Shaowei Jiang. 2025. Heterogeneous prompt-guided entity inferring and distilling for scene-text aware cross-modal retrieval. In *Proceedings of the AAAI Conference on Artificial Intelligence*, volume 39, pages 10537–10545.

Boyuan Zheng, Boyu Gou, Jihyung Kil, Huan Sun, and Yu Su. 2024. [Gpt-4v\(ision\) is a generalist web agent, if grounded.](#)

A Appendix

A.1 Training Configuration

Our training experiments are divided into two stages: supervised fine-tuning (SFT) and reinforcement learning (RL).

A.1.1 Supervised Fine-tuning

For SFT, we follow the training setup and hyperparameter configuration of SeeClick (Cheng et al., 2024) and SimpAgent (Chen et al., 2025). We freeze the visual encoder and fine-tune the model using LoRA, which enables rapid adaptation to GUI tasks. In our preliminary trials, full fine-tuning tended to overfit easily due to the short length of action output. All SFT training details are summarized in Table 7.

Parameter	AC	GUI O	AITW	M2W
global_batch_size	64	64	64	16
total_epochs	3	3	10	3
learning rate	3e-5	3e-4	3e-4	3e-4
lr_scheduler		constant		
lora rank		8		
lora α		16		
lora module		all		
lora dropout		0.1		
warm up		0.01		
bf16		True		
freeze_vision_tower		True		
deepspeed		zero2		

Table 7: Hyperparameters for SFT Training

A.1.2 Reinforcement Learning

For RL training, we follow the Semi-online RL setup in (Lu et al., 2025c). We experiment with two settings: (1) Semi-online RL trained from scratch and (2) Continuing Semi-online RL from an SFT model. The training configurations for different datasets are summarized in Table 8. Same as in (Lu et al., 2025c), our CCPo pipeline first performs SFT on Qwen2.5VL-3B and 7B, and then applies Semi-online RL for further optimization. We run our experiments on 4 nodes, each with 8x NVIDIA H200 GPUs.

A.1.3 Data Preprocessing

To specify our data construction in detail (e.g., using 3AO as the history representation), we generate both the training and evaluation datasets from trajectories starting from 1AO to 3AO turns, limiting the history context to at most 3AO. As a result, the training set contains instances with 1AO, 2AO, and

3AO histories, with 3AO comprising the majority. For a practical and fair comparison, the evaluation set is constructed from the same 1AO–3AO range. This preprocessing pipeline is applied uniformly across all experiments and is used to prepare data for both SFT and RL.

Parameter	AC	GUI O	AITW	M2W
train_batch_size	32	8	16	16
ppo_mini_batch_size	32	8	16	16
total_epochs	3	3	8	8
max_prompt_length	16384	32768	12288	12288
DAPO threshold	0.2	0.1	0.1	0.1
reward discount (SO RL)	0.5	0.3	0.3	0.3
patch threshold (SO RL)			1	
data.max_response_length			128	
truncation			left	
use_kl_in_reward			False	
Advantage weight			1.0	
historical images			1 ~ 5	
learning rate			5×10^{-7}	
fixed_num_mini_batches			4	
ppo_micro_batch_size_per_gpu			1	
kl_loss_coeff			1×10^{-4}	
n_gpus_per_node			8	
nnodes			4	

Table 8: Hyperparameters for Policy Optimization Training

A.2 Agent Tasks

Android Control (Li et al., 2024a) contains 15,283 episodes covering 14,548 unique tasks across 833 Android apps, with an average of 5.5 step actions per episode. We use the official split, 13,604 episodes for training and a test set of 2,855 episodes.

A_{wc} : CLICK, LONG PRESS, SCROLL

A_{nc} : TYPE, HOME, BACK, OPEN, WAIT

GUI Odyssey (Lu et al., 2025a) contains 8,334 cross-app navigation episodes, with an average of 15.3 actions per episode, collected on 6 Android devices, covering 6 task categories, 212 apps, and 1,357 app combinations.

A_{wc} : CLICK, LONG PRESS, SCROLL

A_{nc} : TYPE, PRESS HOME, PRESS BACK, PRESS RECENT, COMPLETE, IMPOSSIBLE

Android In The Wild (Rawles et al., 2023) is a large-scale dataset of human demonstrations for Android devices. It contains 715k interaction episodes and 30k unique instructions, spanning four multi-step subsets. We follow the dataset split of (Cheng et al., 2024) to evaluate models on unseen instructions and avoid overfitting as the split in previous studies.

A_{wc} : CLICK, SCROLL

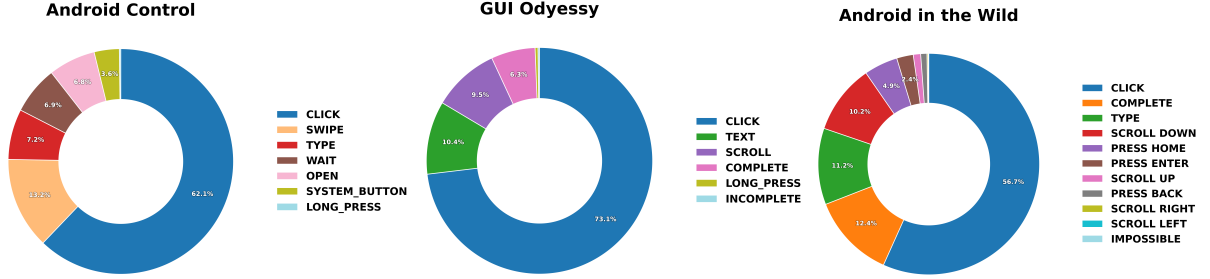


Figure 5: Actions Distribution for Android Control, GUI Odyssey and Android in the Wild dataset

A_{nc} : TYPE, PRESS BACK, PRESS HOME, PRESS ENTER, STATUS TASK COMPLETE, STATUS TASK IMPOSSIBLE

Mind2Web (Deng et al., 2023) is introduced as a real-world web navigation dataset aimed at training and evaluating generalist web agents. It contains more than 2000 open-ended tasks drawn from 137 real websites, where each task comes with a high-level instruction and a human demonstration trajectory. We specifically use the version from (Cheng et al., 2024) for a fair comparison on efficiency, rather than Multimodal Mind2Web from (Zheng et al., 2024).

A_{wc} : CLICK, HOVER, ENTER, TYPE, SELECT

Figure 5 summarizes the action distributions across Android Control, GUI-Odyssey, Android in the Wild, and Mind2Web. A_{wc} accounts for 75% of actions in Android Control, 83% in GUI-Odyssey, and 67% in AITW. In addition, Mind2Web requires coordinate prediction for every action, so A_{wc} accounts for 100%.

A.2.1 Coordinate-Aware Reward Hyperparameters

We analyze the Coordinate-Aware Reward hyperparameter and find that the optimal value of τ_{min} varies across tasks. On the AC and AITW dataset, we compare $\tau_{min} = 0.04$ and $\tau_{min} = 0.1$. Our results indicate that AITW is more challenging and benefits from a larger τ_{min} (e.g., $\tau_{min} = 0.1$). In contrast, a smaller τ_{min} (e.g., $\tau_{min} = 0.04$) can hinder early learning, leading to an approximate 0.2% performance drop. However, for fair comparison and consistency with other datasets, we use $\tau_{min} = 0.04$ in general for all experiments reported in the main paper.

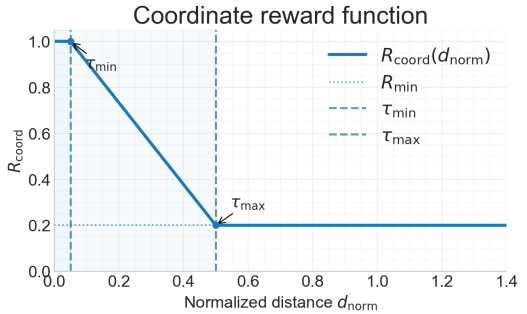


Figure 6: Coordinate-Aware Reward Function

A.3 Ablation Study: A and AO Length Scaling

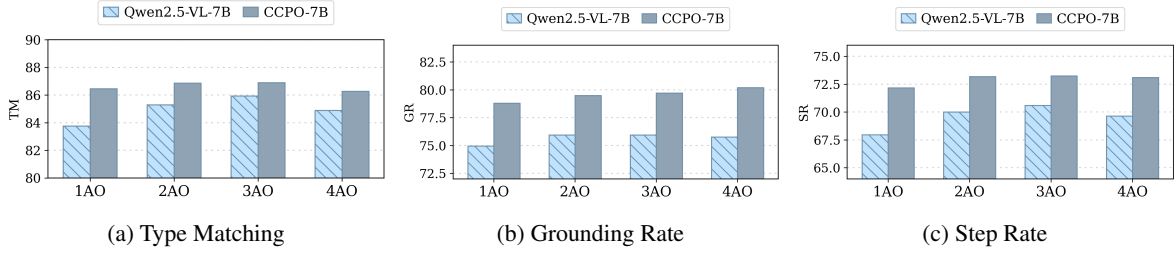


Figure 7: Performance on the AC dataset across different AO.

We analyze the AO setting on the AC datasets and compare different AO lengths by reporting the TM, GR, and SR results in Figure 7 and Table 9. The results indicate that the optimal AO length for AC is around 3 or 4. Notably, for grounding ability, AC with 4AO outperforms 3AO, suggesting that our CCPo effectively improves grounding performance.

Table 16 compares AITW performance across different AO lengths in detail. Our results show that AO length of 5 achieves the best performance. It achieves 1.65% improvement over CCPo-7B-1AO across five subtasks on average.

Beyond the AO settings explored on the AITW and AC datasets, we also evaluate the detailed A and AO settings on GUI Odyssey without CCPo in Figure 8. Since GUI Odyssey involves much longer trajectories than AITW and AC, we investigate action lengths of 2, 4, 8, and 12. Overall, AO consistently outperforms A under the same length setting. However, a longer AO is not necessarily better. We observe that 2A (2AO) achieves performance comparable to 8A (8AO), while 4A (4AO) yields the best results among its tested lengths. This suggests

Model	AO	TM	GR	SR
Qwen2.5-VL-7B	1AO	83.75	74.95	67.97
	2AO	85.30	75.95	70.00
	3AO	85.94	75.95	70.60
	4AO	84.89	75.77	69.65
CCPO-7B	1AO	86.45	78.80	72.18
	2AO	86.86	79.48	73.19
	3AO	86.89	79.71	73.25
	4AO	86.27	80.20	73.11

Table 9: Performance comparison on Android Control from 1AO to 4AO.

that the optimal AO length for GUI Odyssey is around 4 and simply increasing the AO length does not necessarily yield better performance. More broadly, the best choice of A and AO length is task-dependent. However, compressing the historical images efficiently does not degrade performance.

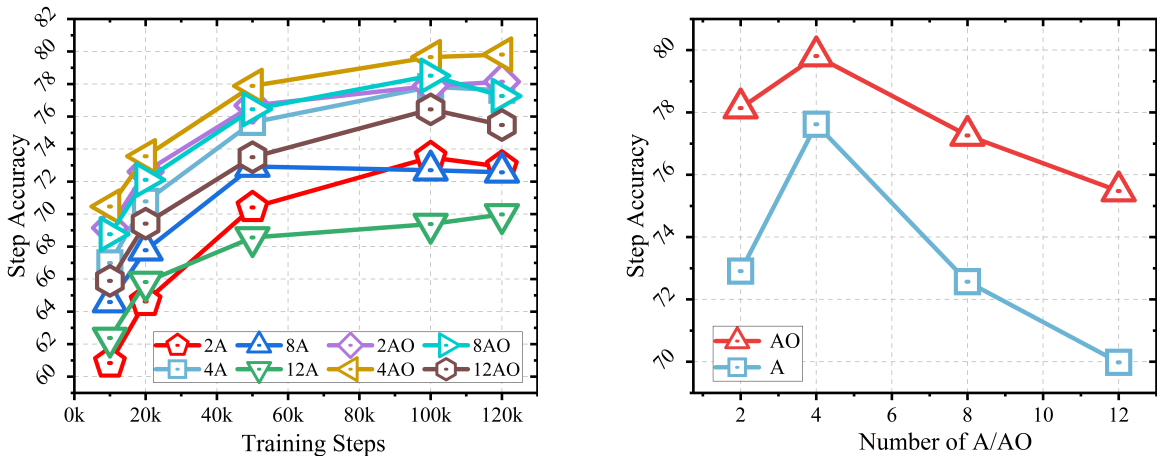


Figure 8: Performance on the GUI Odyssey dataset across different A and AO in SFT training.

A.4 Ablation Study: Compression Variants

Model	Variant	TM	GR	SR	Compression Rate ↑	Step Time ↓
Qwen2.5-VL-7B SO-RL-1AO	ORIG	84.40	75.86	68.62	0.0%	569
CCPO-7B-1AO	MIN	86.50	78.52	72.07	30.6%	327 (1.7×)
CCPO-7B-1AO	MAX	86.45	78.80	72.18	39.3%	186 (3.1×)
Qwen2.5-VL-7B SO-RL-3AO	ORIG	86.26	76.72	70.58	0.0%	717
CCPO-7B-3AO	MIN	86.77	79.32	72.88	37.7%	410 (1.7×)
CCPO-7B-3AO	MAX	86.89	79.71	73.25	53.2%	204 (3.5×)

Table 10: Results on the AC dataset under different compression variants

To better understand how compression affects CCPO performance, we implement two variants: **MAX-COMPRESS** and **MIN-COMPRESS**. **MAX-COMPRESS** is the version we used in the main paper, while **MIN-COMPRESS** is explored as an additional study. The key difference lies in how screenshots from non-coordinate actions are handled:

MAX-COMPRESS: retains only visuals from coordinate-related actions (A_{wc}), discarding all other historical images. **MIN-COMPRESS**: compresses only visuals from coordinate-related actions, leaving visuals from non-coordinate actions (A_{nc}) unchanged.

Empirically, in Table 10, **MIN-COMPRESS** achieves performance close to **MAX-COMPRESS**, with worse grounding ability. However, it yields a worse compression ratio and longer training time. These results suggest that screenshots from non-coordinate actions A_{nc} contribute little to performance. In contrast, coordinate-related visual information appears essential, improving grounding and the overall success rate.

A.5 Ablation Study: Rollout

Since our method progressively aggregates rollouts into trajectories, the number of rollouts is a key hyperparameter that can affect performance.

We evaluate rollout counts of 2, 4, 8, 12, and 16 while keeping the number of training epochs in Table 11. Our results show that a rollout of around 12 performs best on AITW, with 8 also performing strongly. To ensure a fair comparison with prior work (Lu et al., 2025c), we use 8 rollouts for our main results. Notably, larger rollout counts tend to improve performance, likely because more rollouts yield ROI regions that are more precise and estimated with higher confidence.

Model	Rollouts	General	Single	Web Shopping	Install	Google Apps	Overall
CCPO-7B-3AO	2	65.56	78.91	66.63	78.05	77.43	73.31
	4	67.47	79.38	68.48	77.41	77.23	73.99
	8	68.29	78.67	69.62	77.25	78.02	74.37
	12	66.75	79.62	70.57	78.61	77.23	74.56
	16	66.86	79.38	70.33	77.89	77.43	74.38

Table 11: Results comparison on AITW dataset across rollout from 2 to 16.

A.6 Ablation Study: Efficiency

Model	AO	Overall	Token Length	Compression Rate ↑	Step Time ↓
<i>Qwen2.5VL-7B SO-RL</i>	1AO	69.84	2180	0%	140
	2AO	69.74	2613	0%	175
	3AO	69.98	2895	0%	204
	4AO	70.00	2964	0%	213
	5AO	70.53	3065	0%	225
<i>CCPO-7B</i>	1AO	73.47	1463	32.9%	114 (1.2×)
	2AO	73.89	1475	43.5%	116 (1.5×)
	3AO	74.37	1530	46.1%	120 (1.7×)
	4AO	74.80	1555	47.5%	121 (1.8×)
	5AO	75.12	1577	49.3%	128 (1.8×)

Table 12: Performance and efficiency comparison of the Qwen2.5VL-7B Semi-online Reinforcement learning and CCPO-7B model on AITW across 1AO–5AO settings.

We further evaluate efficiency and performance on the AITW dataset (Table 12). Because the AITW images are much smaller than the AC images, the input token sequences are correspondingly shorter. Despite this, the compression rate remains largely unchanged. CCPO maintains a high compression ratio of around 50%, comparable to its compression rate on the AC in Table 15, while still delivering a training speedup of 1.8×. In general, performance improves as compression becomes more effective.

Figure 9 illustrates an important trend in Semi-online reinforcement learning. As the success rate increases, the prompt length tends to grow. Trajectories are rolled out until termination or until the model makes an incorrect prediction, so more accurate agents typically produce longer successful trajectories and therefore longer inputs. In contrast, CCPO can slightly reduce the prompt length over training, benefiting from increasingly accurate predictions. More accurate coordinate predictions enable more aggressive historical image pruning,

which in turn shortens the prompt length.

Finally, we report detailed compression rates and training efficiency on the AC datasets in Table 15. CCPO achieves up to 55% token-length reduction and 3.5 × speedup for 4AO in comparison to original Semi-online RL.

A.6.1 Inference Efficiency

To evaluate the practical deployment potential, we investigate the performance of "optimized inference" (denoted by * in Table 13). Note that while our main experiments strictly follow prior works for fair comparison, this experiment explores the efficiency limit by aligning inference with our training-time CASC. Specifically, Table 13 indicates that resolving the inconsistency between training and inference results in substantial efficiency improvements. CCPO-3AO achieves a 60.0% compression rate, translating to a 2.5× reduction in FLOPs compared to SFT. This confirms that full screenshots contain significant visual noise, and our CASC strategy effectively acts as a denoising mechanism that purifies task-critical information.

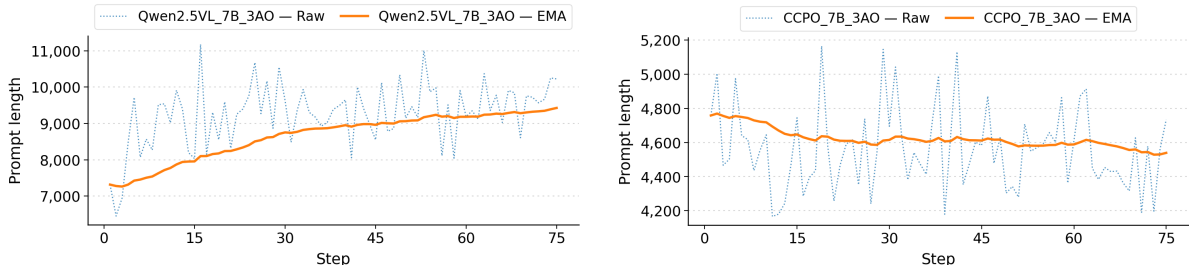


Figure 9: Token length comparison during the training.

Model	M2W-Task	M2W-Domain	M2W-Website	AITW	Token Length	Compression Rate ↑	FLOPs (T)
SFT-1AO	55.60	51.97	51.34	72.32	2662	0.0%	20.75
SFT-3AO	57.30	52.20	54.69	72.89	4293	0.0%	33.05
CCPO-1AO*	56.62	54.53	52.09	73.64	1634	38.6%	12.84 (1.6×)
CCPO-3AO*	57.36	55.14	52.51	73.29	1718	60.0%	13.47 (2.5×)

Table 13: Performance of 7B model with optimized inference on Mind2Web and AITW datasets.

Model	AO	TM	GR	SR	Token Length	Compression Rate ↑	Step Time ↓
<i>Qwen2.5VL-3B</i>	1AO	82.16	74.09	62.94	6998	0%	515
	3AO	83.70	74.78	67.45	9888	0%	660
<i>CCPO-3B</i>	1AO	85.33	76.72	70.60	4271	39.0%	154 (3.3×)
	3AO	85.72	77.49	70.79	4460	54.9%	174 (3.8×)

Table 14: Performance and efficiency comparison of the Qwen2.5VL-3B Semi-online Reinforcement learning and CCPO-3B model on the AC 1AO and 3AO settings.

Model	AO	TM	GR	SR	Token Length	Compression Rate ↑	Step Time ↓
<i>Qwen2.5VL-7B</i>	1AO	84.40	75.86	68.62	7026	0%	569
	2AO	85.05	76.32	70.04	8482	0%	661
	3AO	86.26	76.72	70.58	9550	0%	717
	4AO	85.65	76.74	70.48	10089	0%	760
<i>CCPO-7B</i>	1AO	86.45	78.80	72.18	4263	39.33%	186 (3.1×)
	2AO	86.86	79.48	73.19	4384	48.31%	196 (3.4×)
	3AO	86.89	79.71	73.25	4474	53.15%	204 (3.5×)
	4AO	86.27	80.20	73.11	4531	55.01%	220 (3.5×)

Table 15: Performance and efficiency comparison of the Qwen2.5VL-7B Semi-online Reinforcement learning and CCPO-7B model on the AC across 1AO–4AO settings.

Model	AO	General	Single	Web Shopping	Install	Google Apps	Overall
<i>Qwen2.5VL-7B</i>	1AO	64.85	77.49	68.54	76.86	73.86	72.32
	2AO	65.80	75.83	69.74	77.17	76.04	72.92
	3AO	65.32	76.78	70.04	76.46	75.84	72.89
	4AO	66.51	77.25	70.93	77.41	76.24	73.67
	5AO	66.27	78.67	70.93	77.33	77.23	74.09
<i>CCPO-7B</i>	1AO	66.98	78.20	68.66	77.25	76.24	73.47
	2AO	66.03	78.67	69.86	78.05	76.83	73.89
	3AO	68.29	78.67	69.62	77.25	78.02	74.37
	4AO	68.53	78.91	70.63	77.09	78.81	74.80
	5AO	67.58	78.44	71.35	78.85	79.41	75.12

Table 16: Performance comparison of the Qwen2.5VL-7B SFT and CCPO-7B model on AITW across 1AO–5AO settings.

Method	General	Single	Web Shopping	Install	Google Apps	Overall	ClickAvg
Qwen-VL 9.6B (Bai et al., 2023)	49.5	64.7	50.7	59.9	46.9	54.3	57.4
SeeClick (Cheng et al., 2024)	54.0	73.7	57.6	66.4	54.9	59.3	66.4
R-VLM (Park et al., 2025)	59.9	72.5	61.7	70.6	59.6	64.9	71.0
Qwen2-VL (Bai et al., 2025)	48.3	57.8	51.6	77.4	52.9	57.7	—
Iris (Ge et al., 2025)	61.5	71.4	58.3	66.4	60.2	63.6	71.0
ShowUI-2B (Lin et al., 2024)	63.9	77.5	66.6	72.5	69.7	70.0	—
SimpAgent (Chen et al., 2025)	64.1	76.2	67.2	75.8	74.0	71.5	—
TongUI-3B (Zhang et al., 2025a)	65.6	77.0	65.8	75.1	74.5	71.6	—
TongUI-7B (Zhang et al., 2025a)	67.6	79.9	69.1	76.3	73.5	73.3	—
Qwen2.5-VL-3B w/ SFT	61.52	75.35	67.22	75.81	74.05	70.79	78.42
CCPO-3B 1AO w/o CR	62.71	78.20	65.07	75.50	76.44	71.58	79.12
CCPO-3B 1AO	64.25	76.07	67.22	76.14	75.44	71.83	79.71
CCPO-3B 3AO w/o CR	65.20	79.15	66.63	76.54	75.84	72.67	79.99
CCPO-3B 3AO	65.32	77.49	68.30	78.29	76.04	73.09	80.42
Qwen2.5-VL-7B w/ SFT	64.84	77.48	68.54	76.85	73.86	72.31	80.24
CCPO-7B 1AO w/o CR	66.39	79.38	67.46	75.90	76.24	73.07	79.34
CCPO-7B-1AO	66.98	78.19	68.66	77.25	76.24	<u>73.46</u>	<u>80.98</u>
CCPO-7B 3AO w/o CR	64.85	<u>79.38</u>	69.98	77.25	79.01	74.09	80.52
CCPO-7B-3AO	68.28	78.67	<u>69.61</u>	<u>77.25</u>	<u>78.02</u>	74.37	81.38

Table 17: Evaluation results for CCPO on the AITW benchmark.

Method	Param.	Cross-Task			Cross-Website			Cross-Domain		
		Ele.Acc	Op.F1	Step SR	Ele.Acc	Op.F1	Step SR	Ele.Acc	Op.F1	Step SR
Qwen-VL (Bai et al., 2023)	9.6B	15.9	86.7	13.3	13.2	83.5	9.2	14.1	84.3	12.0
CogAgent (Hong et al., 2024)	18B	22.4	53.0	17.6	18.4	42.4	13.4	20.6	42.0	15.5
SeeClick (Cheng et al., 2024)	9.6B	28.3	87.0	25.5	21.4	80.6	16.4	23.2	84.8	20.8
R-VLM (Park et al., 2025)	9.6B	31.6	88.0	28.7	29.5	84.9	26.1	26.7	85.3	24.3
Iris (Ge et al., 2025)	9.6B	33.5	87.1	32.0	31.2	82.2	26.2	32.8	85.1	28.8
Qwen2-VL (Bai et al., 2025)	2B	51.6	88.6	46.7	48.5	85.7	42.2	48.3	87.0	44.6
ShowUI (Lin et al., 2024)	2B	39.9	88.6	37.2	41.6	83.5	35.1	39.4	86.8	35.2
SimpAgent (Chen et al., 2025)	2B	52.4	89.4	48.7	48.2	85.8	42.2	49.0	88.2	45.0
TongUI-3B (Zhang et al., 2025a)	3B	53.4	89.0	48.8	54.2	86.4	48.1	53.8	88.2	49.5
TongUI-7B (Zhang et al., 2025a)	7B	58.1	88.7	53.4	55.6	87.2	49.0	57.6	88.7	52.9
Qwen2.5-VL 3B 1AO w/SFT	3B	56.61	89.98	52.01	53.31	86.59	46.49	53.00	87.98	48.69
CCPO-3B 1AO	3B	58.66	90.12	54.55	56.52	87.77	50.62	54.51	87.99	50.58
Qwen2.5-VL 3B 3AO w/SFT	3B	57.91	90.98	53.23	53.00	86.89	46.52	53.19	88.75	49.37
CCPO-3B 3AO	3B	61.03	90.95	56.50	58.41	86.61	50.97	56.23	88.80	51.76
Qwen2.5-VL 7B 1AO w/SFT	7B	59.67	90.63	55.60	56.77	88.44	51.34	56.11	88.64	51.97
CCPO-7B 1AO	7B	62.14	91.10	58.00	59.66	86.89	53.41	59.71	90.23	55.66
Qwen2.5-VL 7B 3AO w/SFT	7B	61.92	91.28	57.30	59.10	87.51	52.20	59.03	90.32	54.69
CCPO-7B 3AO	7B	64.31	91.78	59.51	60.14	<u>87.78</u>	<u>53.65</u>	60.79	90.58	56.49

Table 18: Performance comparison on Mind2Web across different settings. We report element accuracy (Ele.Acc), operation F1 (Op.F1), and step success rate (Step SR).

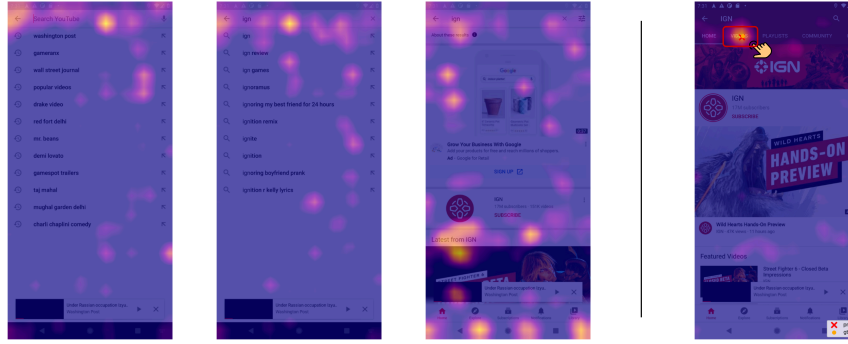
Algorithm 1 CCPO-Style RL Training Loop

Require: Actor policy π_θ , critic V_ϕ , reference policy π_{ref} , reward function r , validation reward r_{val} , training prompts \mathcal{D} , batch size B , epochs E , discount γ , GAE parameter λ , DAPO threshold τ , critic warmup K .

1: Initialization, global step $s \leftarrow 0$
2: **for** $e = 1$ to E **do**
3: **for** mini-batch of prompts $\mathcal{B} \subset \mathcal{D}$ **do**
4: $\mathcal{T} \leftarrow \emptyset$ ▷ accumulated trajectories
5: $n_{\text{prompts}} \leftarrow 0, n_{\text{gen}} \leftarrow 0$
6: **repeat** ▷ multi-round rollouts with coordinate tracking
7: $\tilde{\mathcal{B}} \leftarrow \text{PREPAREBATCH}(\mathcal{B})$
8: ▷ aggregate coordinates from previous steps
9: **for** each trajectory t in $\tilde{\mathcal{B}}$ **do**
10: $g \leftarrow$ example group of t
11: $\mathcal{C}_g \leftarrow \text{AGGREGATECOORDINATES}(g)$ ▷ collect coords from previous resp and ref
12: $\mathcal{B}_g \leftarrow \text{COORDSTOBBOXES}(\mathcal{C}_g)$ ▷ convert to bboxes
13: $\tilde{\mathcal{B}}[t] \leftarrow \text{CROPIIMAGES}(\tilde{\mathcal{B}}[t], \mathcal{B}_g)$ ▷ apply bbox cropping
14: **end for**
15: $\hat{\mathcal{T}} \leftarrow \text{ROLLOUT}(\pi_\theta, \tilde{\mathcal{B}})$
16: $\hat{\mathcal{T}} \leftarrow \text{ACTIONREWARDS}(\hat{\mathcal{T}}, r)$
17: $\hat{\mathcal{T}} \leftarrow \text{COORDSREWARDS}(\hat{\mathcal{T}}, r)$ ▷ compute coords weight
18: **if** KL penalty enabled **then**
19: $\hat{\mathcal{T}} \leftarrow \text{APPLYKLPENALTY}(\hat{\mathcal{T}}, \pi_\theta, \pi_{\text{ref}})$
20: **end if**
21: Update coordinate history from $\hat{\mathcal{T}}$
22: $\mathcal{T} \leftarrow \mathcal{T} \cup \hat{\mathcal{T}}$
23: Update $n_{\text{prompts}}, n_{\text{gen}}$
24: **until** DAPO stopping condition or max generations reached
25: **if** DAPO enabled **then**
26: $\mathcal{T} \leftarrow \text{DAPOFILTER}(\mathcal{T}, \tau, B)$ ▷ keep top- B by DAPO
27: **else**
28: $\mathcal{T} \leftarrow \text{TRUNCATETOBATCHSIZE}(\mathcal{T}, B)$
29: **end if**
30: $\mathcal{T} \leftarrow \text{COMPUTEMASKSANDLENGTHS}(\mathcal{T})$ ▷ build response masks, sequence lengths
31: $\mathcal{T} \leftarrow \mathcal{T} \cup \log \pi_\theta(\text{tokens} \mid \text{inputs})$ ▷ store old log-probs for PPO-style
32: **if** reference policy used **then**
33: $\mathcal{T} \leftarrow \mathcal{T} \cup \log \pi_{\text{ref}}(\text{tokens} \mid \text{inputs})$
34: **end if**
35: **if** critic used **then**
36: $\mathcal{T} \leftarrow \mathcal{T} \cup V_\phi(\text{states})$
37: **end if**
38: $\mathcal{T} \leftarrow \text{COMPUTEADVANTAGES}(\mathcal{T}, \gamma, \lambda, \text{estimator})$ ▷ compute episode level advantages
39: **if** critic used **then**
40: $\phi \leftarrow \text{UPDATERICITIC}(\mathcal{T}, \phi)$
41: **end if**
42: **if** $s \geq K$ **then**
43: $\theta \leftarrow \text{UPDATEACTOR}(\mathcal{T}, \theta)$
44: **end if**
45: $s \leftarrow s + 1$
46: **end for**
47: **end for**
48: **return** π_θ, V_ϕ

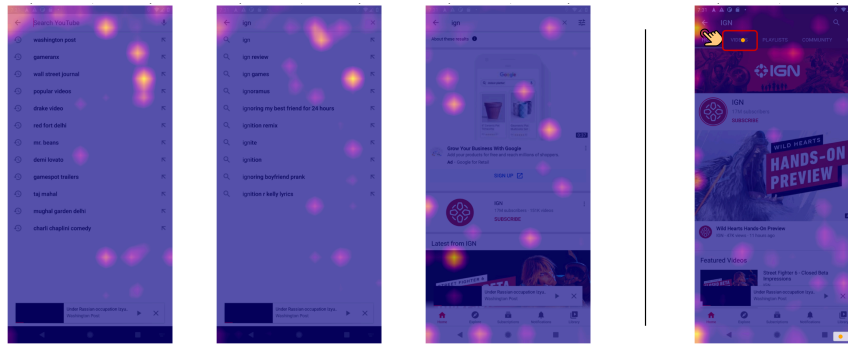
A.7 Use Case

Instruction: What's the latest video from IGN?



(a) CCPo 7B 3AO

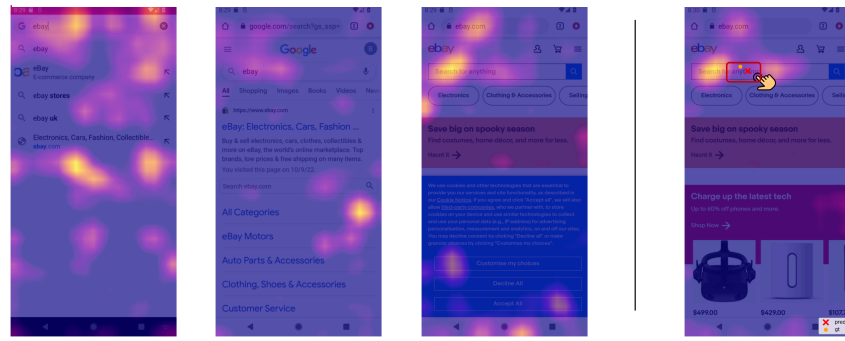
Instruction: What's the latest video from IGN?



(b) Qwen2.5-VL 7B SFT 3AO

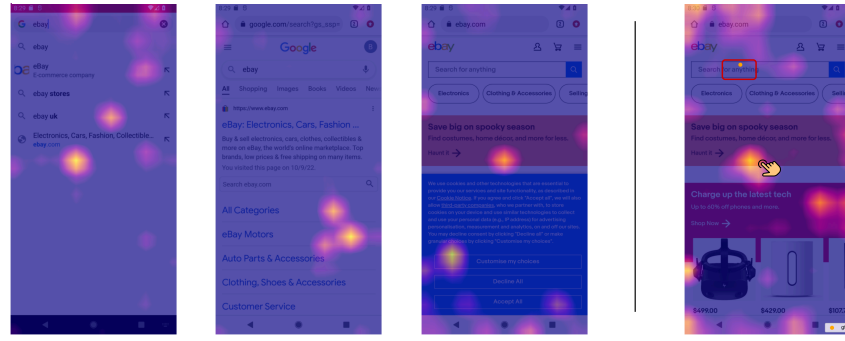
Figure 10: Use case: Attention visualization over the current image and three historical images within a single input.

Instruction: What does the iPhone 8 look like on eBay?



(a) CCPo 7B 3AO

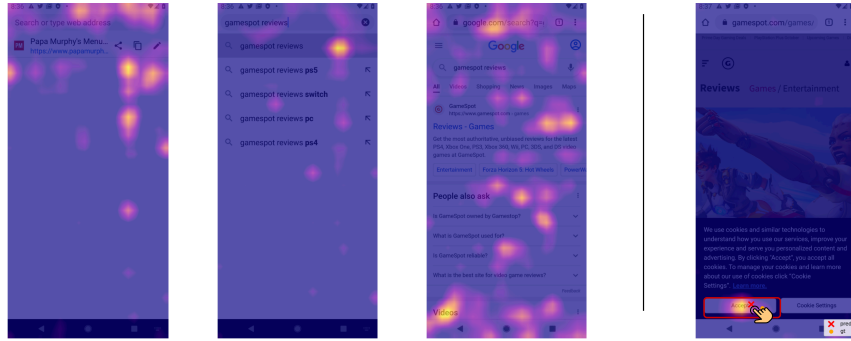
Instruction: What does the iPhone 8 look like on eBay?



(b) Qwen2.5-VL 7B SFT 3AO

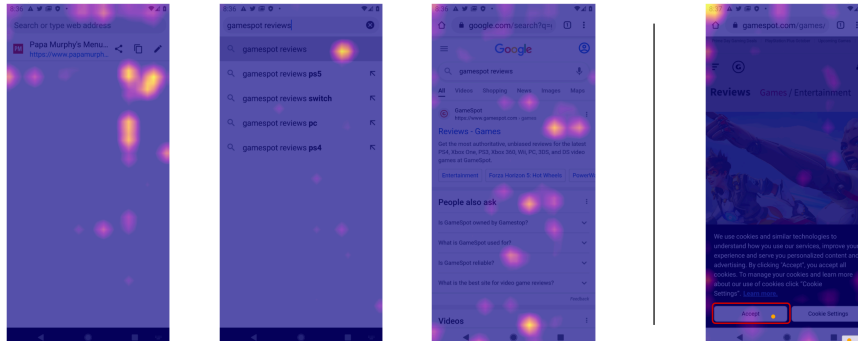
Figure 11: Use case: Attention visualization over the current image and three historical images within a single input.

Instruction: What's the latest video from GameSpot Reviews?



(a) CCP0 7B 3AO

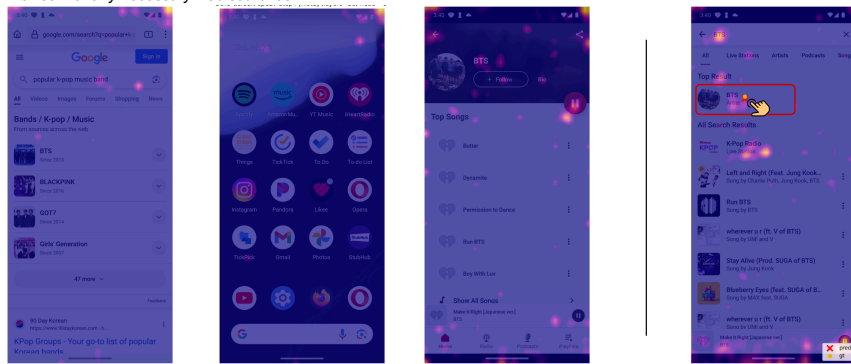
Instruction: What's the latest video from GameSpot Reviews?



(b) Qwen2.5-VL 7B SFT 3AO

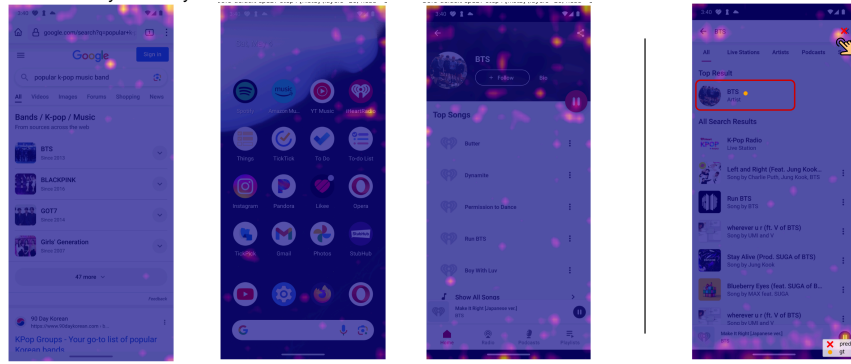
Figure 12: Use case: Attention visualization over the current image and three historical image within a single input.

Instruction: Find a well-known K-Pop band, stream their newest album, and verify the availability of concert tickets. Use 'iHeart: Music, Radio, Podcasts' to listen to the album, 'TickPick - Live Event Tickets' to check ticket availability, and 'Firefox Browser' for any necessary web searches.



(a) CCP0 7B 3AO

Instruction: Find a well-known K-Pop band, stream their newest album, and verify the availability of concert tickets. Use 'iHeart: Music, Radio, Podcasts' to listen to the album, 'TickPick - Live Event Tickets' to check ticket availability, and 'Firefox Browser' for any necessary web searches.



(b) Qwen2.5-VL 7B SFT 3AO

Figure 13: Use case: Attention visualization over the current image and three historical image within a single input.

User Instruction: In the Calculator Unit Converter app and convert 120 Torrs into Pascal units under the pressure tab

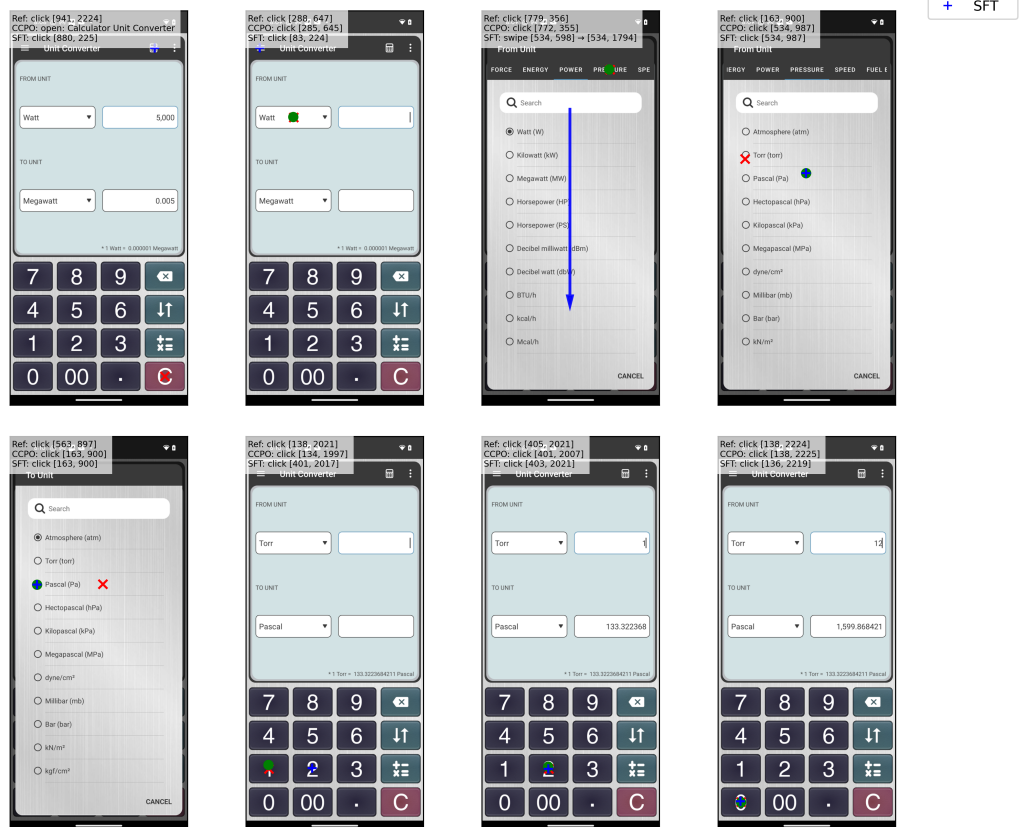


Figure 14: Use case: Full-trajectory examples for CCP0 and SFT.

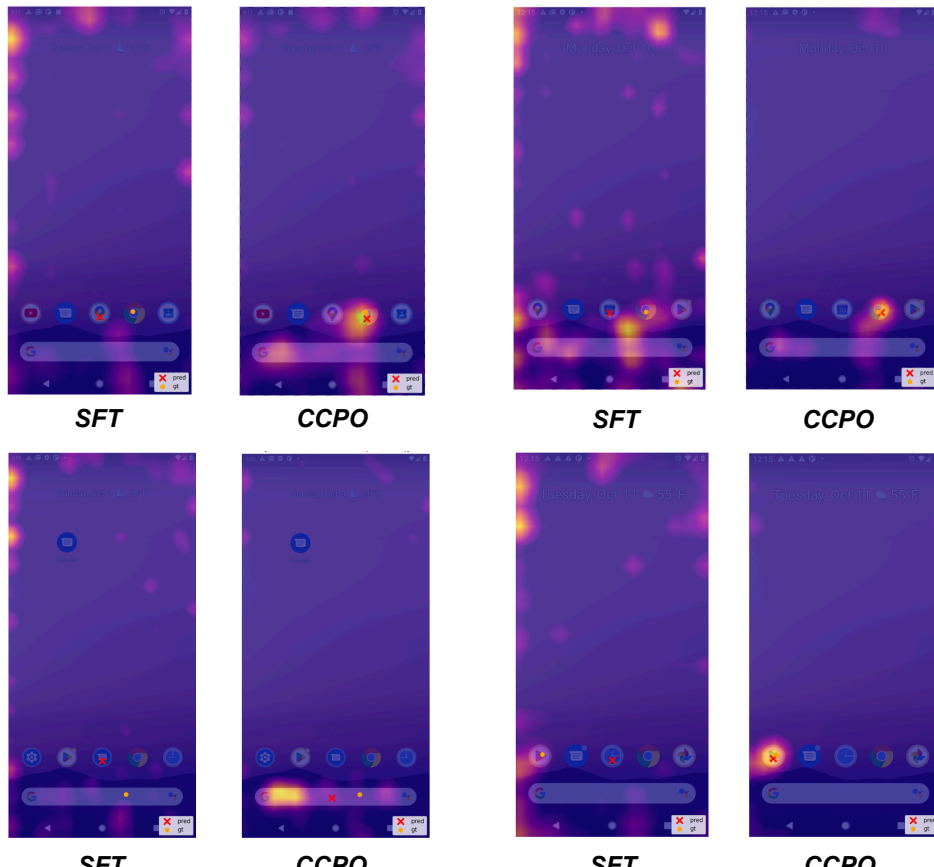


Figure 15: Use case: CCP0 demonstrates improved target-centric attention compared to SFT.

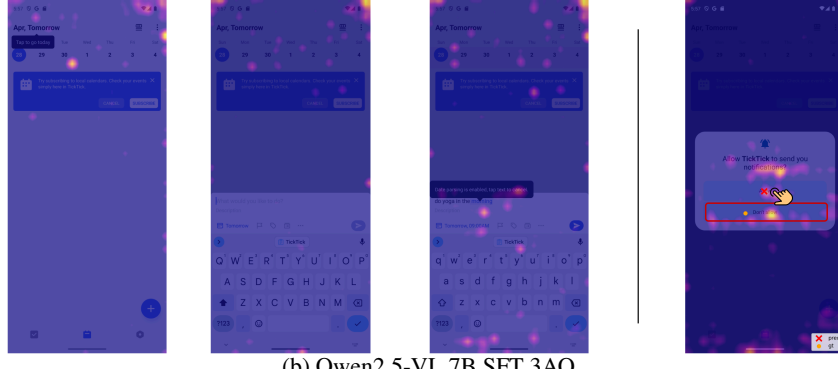
A.8 Failure Case

Instruction: Search for a beginner Yoga workout video on TikTok and set a reminder in TickTick to do it tomorrow morning.



(a) CCPo 7B 3AO

Instruction: Search for a beginner Yoga workout video on TikTok and set a reminder in TickTick to do it tomorrow morning.



(b) Qwen2.5-VL 7B SFT 3AO

Figure 16: Failure case: Attention visualization over the current image and three historical images within a single input.

Instruction: Look up the top video blogs on tech reviews using the Firefox Browser, then increase the brightness on your phone through the Setting app, and finally open YouTube to follow the selected video blogs.



(a) CCPo 7B 3AO

Instruction: Look up the top video blogs on tech reviews using the Firefox Browser, then increase the brightness on your phone through the Setting app, and finally open YouTube to follow the selected video blogs.



(b) Qwen2.5-VL 7B SFT 3AO

Figure 17: Failure case: Attention visualization over the current image and three historical image within a single input.

A.9 Prompt

```
You are a GUI agent. You are given a task and your action history, with screenshots. You need to perform the next action to complete the task.
```

```
## Output Format
```

```
---
```

```
<action> ... </action>
```

```
---
```

```
## Action Space
```

You can perform the following actions:

- key: Perform a key event on the mobile device using adb's `keyevent` syntax.
- click: Click the point on the screen with specified (x, y) coordinates.
- long_press: Press the point on the screen with specified (x, y) coordinates for a specified number of seconds.
- swipe: Swipe from starting point with specified (x, y) coordinates to endpoint with specified (x2, y2) coordinates.
- type: Input the specified text into the activated input box.
- answer: Output the specified answer.
- system_button: Press the specified system button: Back, Home, Menu, or Enter.
- open: Open an application on the device specified by text.
- wait: Wait for a specified number of seconds for changes to occur.
- terminate: Terminate the current task and report its completion status: success or failure.

The arguments you can use are:

- coordinate: (x, y): The x and y pixels coordinates from the left and top edges.
- coordinate2: (x, y): The x and y pixels coordinates from the left and top edges for the endpoint of a swipe.
- text: Text input required by actions like `key`, `type`, `answer`, and `open`.
- time: The time in seconds required by actions like `long_press` and `wait`.
- button: System buttons available for pressing: Back, Home, Menu, or Enter. Possible values: Back, Home, Menu, Enter.
- status: The completion status of a terminated task. Possible values: success, failure.

Format your output as a JSON object with the selected action and its arguments at the same level.

Example outputs:

```
<action>
{"action": "key", "text": "<value>"}
</action>
<action>
{"action": "click", "coordinate": "<value>"}
</action>
```

```
## Note
```

- Planing the task and explain your reasoning step-by-step in `think` part.
- Write your action in the `action` part according to the action space.